Transonic Free-To-Roll Analysis of the F/A-18E and F-35 Configurations

D. Bruce Owens*
NASA Langley Research Center, Hampton, Virginia 23681

Jeffrey K. McConnell†
Lockheed Martin Aeronautics Company, Fort Worth, Texas 76101

Jay M. Brandon‡ and Robert M. Hall‡
NASA Langley Research Center, Hampton, Virginia 23681

The free-to-roll technique is used as a tool for predicting areas of uncommanded lateral motions. Recently, the NASA/Navy/Air Force Abrupt Wing Stall Program extended the use of this technique to the transonic speed regime. Using this technique, this paper evaluates various wing configurations on the pre-production F/A-18E aircraft and the Joint Strike Fighter (F-35) aircraft. The configurations investigated include leading and trailing edge flap deflections, fences, leading edge flap gap seals, and vortex generators. These tests were conducted in the NASA Langley 16-Foot Transonic Tunnel. The analysis used a modification of a figure-of-merit developed during the Abrupt Wing Stall Program to discern configuration effects. The results showed how the figure-of-merit can be used to schedule wing flap deflections to avoid areas of uncommanded lateral motion. The analysis also used both static and dynamic wind tunnel data to provide insight into the uncommanded lateral behavior. The dynamic data was extracted from the time history data using parameter identification techniques. In general, modifications to the pre-production F/A-18E resulted in shifts in angle-of-attack where uncommanded lateral activity occurred. Sealing the gap between the inboard and outboard leading-edge flaps on the Navy version of the F-35 eliminated uncommanded lateral activity or delayed the activity to a higher angle-of-attack.

Nomenclature

b_{ref}	=	reference wing span
C_L	=	lift coefficient
C_l	=	rolling moment coefficient
C_{lrms}	=	rolling moment coefficient root mean square
c_{ref}	=	reference wing chord (mean geometric chord)
CBSTAT	=	Continuous Beta Sweep Test and Analysis Technique
CTOL	=	Conventional Take-Off and Landing
CV	=	Carrier Version
FTR	=	free-to-roll
LE	=	leading edge
LEF	=	leading edge flap
M	=	Mach number
p_{P-V}	=	free-to-roll figure of merit
Re	=	Reynolds Number based on c_{ref}
S	=	reference surface area
t	=	time
TEF	=	trailing edge flap
V_∞	=	freestream velocity
VG	=	vortex generator
α	=	angle of attack
β	=	angle of sideslip

*Aerospace Engineer, Associate Fellow AIAA
†Aeronautical Senior Staff Engineer, AIAA member
‡Senior Research Engineer, Associate Fellow AIAA
Approved for Public Release, SPR-118.04

δ_{ailF} = aileron deflection where both left and right ailerons are deflected symmetrically
δ_e = symmetric horizontal tail deflection
δ_{LEF} = leading edge flap deflection
δ_{ILEF} = inboard leading edge flap deflection
δ_{OLEF} = outboard leading edge flap deflection
δ_{TEF} = trailing edge flap deflection
ϕ = roll angle
ϕ_o = initial roll angle
$\dot{\phi}$ = roll rate, time derivative of the roll angle
$\ddot{\phi}$ = roll acceleration, time derivative of the roll rate
θ = pitch angle

I. Introduction

Uncommanded lateral motions (wing drop/rock) plague many aircraft both in the low-speed high angle of attack (AoA) and high-speed moderate AoA flight regimes[1]. The FTR technique has been used for many decades to address the low-speed problems at a number of test facilities. Application of FTR in the transonic regime has been much more limited but some testing was performed in Russia at the Sibnia Aerodynamic Research and Development Division[2] and in a semi-free-to-roll test conducted by Northrop and NASA Ames for the F-5A[3]. More recently the NASA/Navy/Air Force Abrupt Wing Stall (AWS) Program used the technique to assess uncommanded lateral activity on four military aircraft. The results of these free-to-roll tests as well as static force and moment, CFD, simulation, and flight tests are reported in Refs. 4-21.

During the three-year Engineering and Manufacturing Development (EMD) flight test program the pre-production F/A-18E/F aircraft experienced wing drop during wind-up/down turns in the high subsonic/transonic flight regime. The majority (so-called 80% solution) of the wing drops were eliminated by rescheduling the flaps (v6.1.3 control laws). The remaining "20%" of the problem was resolved by replacing the solid wing fold fairing with a porous fairing. Even so, it was recognized that the flying qualities could still be improved. To address this issue, additional wind tunnel and flight testing was performed by a Boeing/Navy Transonic Flying Qualities Improvement (TFQI) team. In flight tests, it was found that a saw-tooth LEF and two fences located on the wing box inboard of the wing fold was equal to or better than the original solution in terms of the overall transonic flying qualities. This configuration will be called SW2F in this paper. This paper will analyze the SW2F configuration using static force & moment and FTR data. The SW2F configuration was tested using an 8% F/A-18E model in the NASA LaRC 16-Foot Transonic Tunnel (16-ft TT) during the AWS dynamic test technique evaluation.

The current analysis will focus on the use of wind tunnel data to identify configurations that improve lateral transonic flying qualities. The ideal case would be to use the wind tunnel data results, along with data derived from CFD and other analytical sources to model the unsteady aerodynamics for a piloted simulation study. This type of analysis, as recommended by Cook, et al.[20], would give a more comprehensive assessment of the flying qualities but is beyond the scope of this paper. In pre-production F/A-18E/F flight tests, after conducting the maneuver, pilots would assess the lateral activity immediately after completing a maneuver using a stoplight rating.[15] The transonic wind-up turns were mainly conducted for $0.7 \le M \le 0.95$ at altitudes between 2.5K and 25K. Turns were conducted using a relatively slow pull up to the maximum allowable load factor. The maximum AoA during the maneuver would be between 15° and 20° with a maximum LEF deflection of approximately 20°. With the v6.1.3 flap schedule, the region of residual uncommanded lateral activity normally occurred at LEF values between 10° and 15° so these two flap deflections were selected for wind tunnel testing. The analysis will compare the SW2F configuration to a baseline which has the same δ_{LEF} , δ_{TEF} , and δ_{ailF} as the SW2F configuration but without the saw-tooth LEF and the fences. The analysis will draw upon all of the available data to draw conclusions.

Early in the System Demonstration and Development (SDD) phase of the F-35 Joint Strike Fighter (JSF) Navy variant, several warning signs were seen in the static wind tunnel data indicating the potential for wing drop at transonic Mach numbers. These signs included abrupt shifts in rolling moment, lift inflections, rolling moment offsets, and poor data repeatability. Based on these observations, Lockheed Martin began coordinating closely with the ongoing AWS effort to take full advantage of the knowledge and expertise that had been developed as part of that program. Since the F-35 program was in the midst of an extensive wind tunnel test program at that time, one particularly relevant aspect of the AWS program was the research done to develop a reliable technique for predicting wing drop from static wind tunnel testing. The need for such a technique was highlighted during the pre-production F/A-18E/F program where the lack of a reliable wind tunnel based method for predicting wing drop forced the

evaluation of potential fixes to be done almost entirely through flight test. Although several static wind tunnel based figures of merit were evaluated under the AWS program, this effort met with only limited success. By contrast, the transonic FTR technique, also developed under the AWS program, provided outstanding correlation to flight test results for a range of configurations. Ultimately, the AWS program recommendation was to use FTR as the primary means of verifying that a new aircraft design is wing drop free.

Unfortunately, static wind tunnel testing was the only practical method for performing rapid aerodynamic evaluation available to the JSF program given the number of configurations and the range of flight conditions to be considered. With this in mind, Lockheed Martin elected to channel resources into developing a technique for identifying potential wing drop problems based solely on conventional force and moment testing. The end result of this effort is the Continuous Beta Sweep Test & Analysis Technique (CBSTAT) which is described in detail in Ref 22. Using CBSTAT as the primary evaluation criteria, several potential design options were investigated to help understand and correct the aerodynamic deficiencies seen in the transonic Mach, moderate AoA flight regime. The source of the problem was eventually traced to a gap between the inboard and outboard LEF at the wing fold. An aircraft level trade study was then launched to identify and implement potential fixes. This study led to a modification of the CV LEF arrangement that allowed the gap to be sealed in flight while maintaining the required wing fold capability. Subsequent CBSTAT based evaluations of the modified configuration indicated that the sealed gap successfully resolved the wing drop concerns. However, since previous efforts to establish a correlation between static test based wing drop predictions and flight test results had been unsuccessful, additional verification of the proposed solution was warranted. A FTR test was therefore added to the JSF test program to validate CBSTAT and to confirm that the configuration changes made to the CV variant did improve the lateral characteristics. To further explore the validity of CBSTAT, it was also applied to the pre-production F/A-18E and Harrier II configurations in separate wind tunnel tests. The analyses of these wind tunnel tests are presented in Ref. 23 and 24. Reference 25 presents the correlation of CBSTAT and FTR to flight test results.

The objective of this paper is to analyze the effect of configuration changes on the lateral activity of an 8% F/A-18E and 1/15th scale F-35 aircraft models using the FTR technique at transonic speeds. For the F/A-18E model, a modification to the LEF shape at the wing fold fairing location and wing-box fences will be compared to a baseline configuration. For the JSF model, data for both the CTOL and CV variants will be analyzed with special emphasis on how the modified CV wing compares to the baseline configuration. The paper will show only aerodynamic effects because control system effects were not modeled. The time histories of the uncommanded lateral activity will be analyzed using static force and moment data as measured by the internally mounted six-component strain gauge balance and dynamic data extracted from the roll angle time histories using parameter identification (PID) methods.

II. FTR Test Technique

The FTR test technique is a single-degree-of-freedom method where the model is constrained to roll about the longitudinal body axis. When testing in this mode the rotary section of the FTR rig, the sting, the balance, and the model all rotate on two sets of low friction bearings in response to the aerodynamic rolling moments exerted on the model. The rolling motion can be described by a combination of forcing functions, roll damping, (C_{lp}), and lateral stability ($C_{l\beta}$) effects. Therefore, it is instructive when analyzing the data from a FTR test to consider the equation of motion in terms of the Euler angle ϕ as: $\frac{I_x\ddot{\phi}}{qSb} - C_{l_{\dot{\phi}}}\frac{\dot{\phi}b}{2V_\infty} - C_{l_\phi}\phi = C_{l_o}$. The foregoing equation is in the form of the classical mass-spring-damper system where: C_{lo} represents an aerodynamic forcing function; C_{l_ϕ} represents the spring constant which, along with the inertia, determines the frequency of oscillation; and $C_{l_{\dot{\phi}}}$ represents the damping coefficient. In the FTR technique, the use of $C_{l_{\dot{\phi}}}$ and C_{lp} is kinematically equivalent. By measuring roll angle versus time, the FTR technique captures the composite effect of both static and dynamic forces acting on the model regardless of whether they are steady or unsteady.

The top-level analysis from FTR testing involves assessing the severity of lateral activity. Since the models are typically not dynamically scaled it is difficult to draw the line between acceptable and unacceptable lateral activity based solely on the behavior of the model. Therefore the severity of the lateral activity is assessed using the flight data correlated FTR FOM that was developed during the AWS program[14]. The FTR FOM is computed from a time history of the roll angle using the following procedure. First, the absolute value of the amplitude change from a local maximum (peak) to its nearest local minimum (valley) is determined. Then, this value is divided by the time it takes to roll through this amplitude change. This ratio is, of course, the slope of a line connecting the maximum to

the subsequent minimum. This quotient is computed for all of the maximums and minimums in a time history and the final FTR FOM, $p_{p\text{-}v}$, is selected as the highest of these ratios. In Ref. 14 this ratio was retained as a dimensional number but for this paper the ratio is nondimensionalized using $b/2V_\infty$ to make the acceptable thresholds more generally applicable. Mathematically stated as: $p_{P-V} \equiv \left(\left| \frac{\Delta\phi}{\Delta t} \right| \frac{b}{2V_\infty} \right)_{\max}$ the threshold for this figure of merit was established as $p_{p\text{-}v} > 0.002$ through correlation to flight data that showed significant lateral activity. This FOM is not intended to indicate the type of motion, how long it took for the motion to develop or how often the events happened. However it has proven to be an accurate indicator of where uncommanded lateral motion will occur in flight and serves as conservative first filter for assessing the severity of the motion.

In practice, the FTR technique is an extension of static force and moment testing. The technique is used to evaluate the unsteady aerodynamic effects that time averaged static force and moment data do not accurately capture. Also, the FTR technique captures roll damping effects that cannot be obtained in static testing. The primary data from the FTR technique is the roll angle time history from which roll rate and roll acceleration can be determined. Knowing the roll acceleration and the inertia of the system the total aerodynamic rolling moment can be computed. Of the static data, $C_l(\beta)$ or $C_l(\phi)$ are the most useful for understanding the FTR motions. These data indicate rolling moment forcing functions and lateral stability (spring) effects. When available, C_{lrms} data can provide insight into the level of unsteadiness but does not quantify rolling moment rate of change. The lift curve indicates areas where the wing flow topology is changing. It tells at what α the wing*s* are stalling. It does not tell if the stall is asymmetric. If a rolling moment offset is at the same α as wing stall then the probability of a lateral motion is increased. If the lateral activity occurs during significant reduction in lift (i.e. a negative lift curve slope), then a loss in roll damping can be expected. Therefore, the FTR and static tests are collaborated to provide a better understanding of the uncommanded lateral activity.

Since friction and inertia tend to subdue the lateral motion during FTR testing, efforts are made to minimize these effects. Large inertia about the roll axis makes the model less sensitive to changes in lateral aerodynamic asymmetries making it difficult to resolve differences in configurations with small values of $p_{p\text{-}v}$. The effect of friction is to add artificial damping to the system. The FTR rig is designed to minimize friction but this force is difficult to predict or model because it tends to be a function of the force acting normal to the roll axis bearings. Efforts have been made to quantify the friction effects but thus far the accuracy of these calculations has not been entirely satisfactory. A separate research effort has been initiated to address the friction issues.

III. Wind Tunnel Tests

A. Models

An 8% scale model of the pre-production F/A-18E (Fig. 1) and a 1/15th scale model of the JSF (Fig. 2) were tested in the NASA Langley 16-Foot Transonic Tunnel. The models were not dynamically scaled. The issues of dynamic scaling are addressed in Refs. 14, 26, and 27. The pre-production F/A-18E FTR test was conducted as part of the AWS program during the spring of 2002. The JSF FTR test was conducted during February and March of 2003.

The 8% pre-production F/A-18E was tested in a baseline and modified configuration. The model did not incorporate the porous wing fold fairing. Two sets of flap deflections were used in the test. In the discussion, a flap set for the pre-production F/A-18E is denoted as: $\delta_{LEF}/\delta_{TEF}/\delta_{ailF}$ in degrees. The flap deflections used were 10/10/5 and 15/10/5. The ailerons are deflected symmetrically as flaps. The flap sets tested corresponded to those used in representative flight maneuvers. The modification to the baseline changed the LEF snag to a saw-tooth shape and placed two wing-box fences at the spanwise locations as shown in the sketch of Fig. 3. A picture of the saw-tooth and fences are shown in Fig. 4. The configurations were tested at $M = 0.80$ and 0.90 with $Re = 4$ million based on c_{ref}.

The CTOL and CV variants of the JSF model were tested. No variations to the CTOL model were tested but numerous modifications to the CV model were assessed. On the CV model, the baseline wing had an inboard and outboard LEF that had different hinge-lines (see Fig. 2). When the LEF was deflected, the outboard section would be at a higher deflection than the inboard and will be denoted in the discussion as $\delta_{LEFI}/\delta_{LEFO}$ in degrees. The LEF deflections tested on the baseline wing were: 10/12.4, 12.5/15.5, 16/19.8, and 20/24.8. . There was also a gap between the inboard and outboard LEF sections on the baseline CV such that the two were not touching and moved independently. Prior to the FTR test, CBSTAT evaluation showed that sealing this gap eliminated deficiencies in the static lateral characteristics which were considered to be indicators of wing drop. To facilitate the closing of this gap a modification to the configuration was developed which involved using a common hinge-line for both the

inboard and outboard flap and maintaining equivalent deflections. To model this in the wind tunnel, separate parts were used for the inboard and outboard LEFs but the gap was sealed with dental plaster and tape. This non-permanent seal was selected to permit investigations to be conducted with the gap open, partially open and fully sealed. The wing with the common hinge-line and sealed gap, which will simply be referred to as the "new wing", was tested at LEF deflections of 10°, 12°, and 16°.

Many other parameters were varied during the JSF testing to understand the influence of various configuration changes. These parameters included TE flap deflection, symmetric aileron deflection, horizontal-tail deflection, VG arrays on the outer wing panels, removing the transition trip dots, and beveling the inboard face of the outboard LEF. The model was tested over the speed range $0.60 \le M \le 0.98$ with a corresponding Reynolds number variation of 3.7 to 4.1 million based on c_{ref}.

The 16-ft TT wind tunnel tests consisted of a static force and moment phase and a FTR phase. For both phases the models were tested on the FTR rig as shown in Fig. 5. During the static force and moment testing, a locking bar was placed across the stationary and rotary sections of the FTR rig and data were measured using an internally mounted six-component strain-gauge balance. The static data were taken in a point-pause mode. In this mode the model is held at a fixed condition, 50 samples are acquired over a 5 second window then averaged to create a single data point. This paper also presents data from a JSF static force & moment test conducted in the Veridian Transonic Wind Tunnel. These data were also measured using an internally mounted six-component strain gauge balance but were acquired during continuous β-sweeps performed at a sweep rate of 0.33°/sec.

During the 16-ft TT FTR tests, the roll angle time history was measured using a resolver with an accuracy of 0.067°. The roll angle signal was captured at a rate of 200 Hz using a 4 Hz analog filter. The strain-gauge balance signals were recorded at 50 Hz using a 10 Hz analog filter and, video of the rolling motions was recorded.

During the FTR test phase, three test methods are employed to investigate the potential for lateral activity: continuous pitch sweep, pitch-pause with $\phi_o = 0°$ and pitch-pause with $\phi_o \neq 0°$. Reference 14 provides a detailed description of the procedures for conducting FTR testing using each of these methods. Unlike static force and moment testing where α and β are standard model attitude variables, FTR testing uses θ and ϕ as the primary independent variables. When the parameter α is used to compare static and FTR data, without stating a specific β, then it is implied that $\beta = 0°$ in both types of data.

B. Roll Damping Derivative Estimation Method

The roll damping derivative, C_{lp}, given in this paper was estimated using PID methods. The method used in the current analysis is based on linear regression performed using a package of MATLAB® scripts developed at NASA Langley called SIDPAC[28]. The FTR motions are modeled in this approach using the governing equation given above assuming constant coefficients over a specified range of ϕ. Also, note that the actual parameter that is being computed is $C_{l_p} + C_{l_{\dot{\beta}}} \sin\alpha$ due to the body axis motion

IV. Results and Discussion

The discussion of the pre-production F/A-18E will show results of two different flap sets – 10/10/5 and 15/10/5 – at Mach numbers of 0.8 and 0.9. The FTR FOM will be the starting point for the discussion with the use of static and dynamic data to explain the effect of adding the saw-tooth and fences to the baseline. In the discussion of the pre-production F/A-18E data, $C_{l\beta}(\alpha,\beta=0°)$ will be used to succinctly discuss the static lateral stability over the α-range used in the test. The rolling moment data from β-sweeps were used to verify that this representation of the static lateral stability is accurate enough for the current discussion. After the pre-production F/A-18E results, the JSF data will be presented for the CTOL and CV variants. For the CV variant, the data will show the effect of sealing the LEF gap at the wing fold junction, partially sealing this gap, vortex generators, beveling the inboard face of the outboard LEF, the effect of deflecting the horizontal tail, and the use of $p_{p\text{-}v}$ for flap scheduling.

A. Pre-production F/A-18E

1. Configuration 10/10/5; M = 0.8

The lateral activity of the baseline and SW2F configurations are shown using the FTR FOM in Fig. 6. The baseline has significant activity at $\alpha = 8°$, 8.5°, and 10°. The SW2F has significant activity for $9° \le \alpha \le 10°$ and $\alpha = 15°$. The roll angle time histories during continuous pitch-up sweeps for the two configurations are shown in Fig. 7. The figure shows that the SW2F delays the α at which significant lateral activity begins by 1° beyond the baseline. Unfortunately, the lateral activity that does result is very severe. The time histories also show that both

configurations have a sudden roll off around $\alpha = 15°$. The lateral motion observed in these time histories will be explained in the following discussion.

From roll angle time histories during pitch-pause points both with $\phi_o = 0°$ and $\phi_o \neq 0°$ (not shown), the lateral activity for the baseline configuration at $\alpha = 8°$ and 8.5° is mild occasional wing rock. The lateral activity at $\alpha = 10°$ occurs more often than at $\alpha = 8°$ and 8.5° with a slightly larger amplitude but the same frequency. This constant frequency agrees with the constant values $C_{l\beta}$ over this α-range as shown in Fig. 8. The increase in $p_{p\text{-}v}$ at $\alpha = 10°$ is caused by the increase in amplitude since the frequency stayed the same.

The type of lateral motion for the SW2F configuration at the same points of significant lateral activity was notably different. There was no significant activity during the pitch-pause points with $\phi_o = 0°$, except at $\alpha = 15°$. The significant activity in the $9° \leq \alpha \leq 10°$ range as identified by the FTR FOM *only* occurred if the model was given a roll rate. The pitch-pause points with $\phi_o \neq 0°$ (see Fig. 9 for example) show that the model will exhibit violent varying amplitude wing rock for the $9° \leq \alpha \leq 10°$ range.

The pitch-pause point (see Fig. 10) and continuous pitch-up sweeps show that the lateral activity for $\alpha = 15°$ is simply an abrupt trim change wings level to $\phi = 20°$. No wing drop/rock occurs about the $\phi = 20°$ trim point. The value of $p_{p\text{-}v}$ for this point is caused by this trim change.

A more complete understanding of the rolling motion types for the two configurations can be made by using the static force & moment data along with the FTR data. The lift curve of Fig. 11 shows that the baseline wing is going through stall between $\alpha = 7°$ and 10°. The stall is gradual and $C_{L\alpha}$ is always positive. In contrast, the SW2F configuration does not stall as gradually and exhibits a sharp negative $C_{L\alpha}$ break at $\alpha = 9°$. The lift curves are practically identical for $\alpha \geq 9.5°$. The type of wing stall exhibited by the SW2F configuration increases the chance of a loss in roll damping. The C_{lp} data for the SW2F of Fig. 12 shows a loss of roll damping at stall. The static rolling moment data for the baseline configuration (Fig. 13) shows a small rolling moment offset while the wing is going through stall. The significant amount of C_{lrms} through the wing stall (Fig. 14), however, indicates the flow is unsteady. The rolling moment data for the SW2F configuration in Fig. 13 shows slightly more rolling moment offset than the baseline but the offset is small. The C_{lrms} for the SW2F configuration is much less than the baseline. Therefore, the mild wing rock of the baseline configuration is caused by unsteady rolling moment offsets as the wing goes through stall while the SW2F lateral activity is caused by a loss in roll damping.

The lateral activity at $\alpha = 15°$ for the SW2F configuration demonstrates the effect of unstable $C_{l\beta}$ on the lateral characteristics. Figure 8 shows the static lateral stability for the two configurations. At $\alpha = 15°$ the SW2F configuration suddenly goes statically unstable. The continuous pitch-up sweep data of Fig. 7 and the pitch-pause point with $\phi_o = 0°$ data of Fig. 10 shows that model is well damped. But, the rolling motion is such that model simply locks in to a $\phi = 20°$ trim point after three monotonically decreasing overshoots. The static rolling moment data for the SW2F configuration for $\beta = 0°$ shown in Fig. 13 shows a large rolling moment spike of ~0.012 at $\alpha = 15°$. Large rolling moment spikes of this magnitude have been thought to be associated with significant wing drop. The $p_{p\text{-}v}$ for this point, however, is relatively small illustrating the value of the FTR technique in discerning the effect of large rolling moment offsets. A large rolling moment spike does not imply that a significant wing drop will occur.

In summary, the effect of adding the saw-tooth and fences was to delay the α-onset of lateral activity by 1°, increase $C_{l\beta}$ and reduce roll damping during the stall, and reduce the rolling moment unsteadiness. Also, the analysis showed that wing drop/rock is more violent when $C_{l\beta}$ (the spring) is strong. Finally, it showed the value of the FTR technique in discerning the effect of large rolling moment offsets.

2. Configuration 10/10/5; M = 0.9

The lateral activity of the baseline and SW2F configurations for $M = 0.9$ are shown using the FTR FOM in Fig. 15. The baseline has significant activity at $8° \leq \alpha \leq 9°$, and 10°. The SW2F has significant activity for $\alpha = 7°$ and $10.5° \leq \alpha \leq 11.2°$. Up to $\alpha = 10°$, the baseline configuration exhibited slow aperiodic motion with no sharp wing drops. The SW2F configuration exhibited increased static lateral stability and roll damping relative to the baseline through $\alpha = 10.5°$. This improvement in the static and dynamic lateral stability was enough to decrease the severity of the motion below the threshold of significant activity except at $\alpha = 7°$. As with the other SW2F Mach and flap configurations, the SW2F has a sudden loss in roll damping at wing stall but strong $C_{l\beta}$. Therefore, in the $10.5° \leq \alpha \leq 11.2°$ range the SW2F exhibited large amplitude violent wing rock if the model was given a roll rate.

As mentioned above, there was significant lateral activity for the SW2F configuration at $\alpha = 7°$. The time history of the model at this α is shown in Fig. 16. As shown in the Fig., the level of $p_{p\text{-}v}$ is due to the single 30° wing drop at $t = 20$ sec. out of over 60 seconds. Even though the amplitude of the drop is large the rate is relatively

slow. This results in a value of $p_{p\text{-}v}$ that is barely above the threshold of significant lateral activity. Also, the drop is highly damped with only one overshoot of 10° amplitude. The C_l, C_{lrms}, $C_{l\beta}$, C_{lp}, and C_L data (not shown) give no indication why this wing drop occurred. Also, this point was repeated with no wing drop occurring. Therefore, it is judged that this point would not be a problem in flight. This point also demonstrates that the FTR FOM acts as a conservative first filter for identifying potential lateral activity but should not be used as the only indicator. It is only after careful consideration of all available data (static and dynamic) that the potential for lateral activity can be judged accurately.

3. Configuration 15/10/5; M = 0.8

The level of lateral activity for the baseline and SW2F configurations are shown using the FTR FOM in Fig. 17. The baseline has significant activity at $8° \le \alpha \le 10°$. The SW2F has significant activity for $8.5° \le \alpha \le 11°$. The type of motion is approximately the same for both configurations – occasional lightly-damped wing drop. The α-onset of motion for the SW2F configuration is delayed by 0.5 degrees. The static force and moment data support the motion seen on the FTR rig. In summary, both configurations have the same type of lateral activity at nearly the same levels. The difference being that the SW2F delayed the α-onset of activity by 0.5°.

4. Configuration 15/10/5; M = 0.9

The lateral activity of the baseline and SW2F configurations for $M = 0.9$ are shown using the FTR FOM in Fig. 18. From the results of this figure the lateral activity will be discussed in two separate α regions: $4° \le \alpha \le 11°$and $\alpha > 11°$. The static force and moment data will be used to explain the activity.

The data show that through $\alpha = 11°$ the baseline and SW2F configurations had approximately the same levels of lateral activity. Between $5.5° \le \alpha \le 12.5°$ the static rolling moment data (Fig. 19) was different for the two configurations but have similar variances. The variations were the range $C_l = \pm 0.002$. For $5.5° \le \alpha < 10°$, the SW2F configuration has an increase in static (Fig. 20) and dynamic (Fig. 21) lateral stability over the baseline. The roll angle time history for the baseline and SW2F configurations during a continuous pitch-up sweep are shown in Fig. 22. Comparing the first 55 seconds of the baseline configuration (at $t = 55$s, $\alpha \sim 11°$) to the first 45 seconds of the SW2F configuration (at $t = 50$s, $\alpha \sim 11°$) graphically demonstrates the effect of the rolling moment offsets and static and dynamic lateral stability shown in Figs. 19 and 20, respectively. The lateral activity significantly changes between the two configurations above $\alpha = 11°$. The lateral activity was benign for the baseline in this α-range. The SW2F configuration has mild to moderate lateral activity in the $11° < \alpha < 12°$ range and then violent lateral behavior in the range $13° < \alpha \le 14°$. There is a spike in the static rolling moment data at $\alpha = 13.5°$ but the values $p_{p\text{-}v}$ in the $13° < \alpha \le 14°$ range only resulted from when the model was given a roll rate. In other words, the values of $p_{p\text{-}v}$ did not occur from uncommanded lateral activity. In this same α-range the SW2F configuration exhibited a loss in roll damping while maintaining a strong $C_{l\beta}$. Therefore, the level of lateral activity in the $13° < \alpha \le 14°$ range is due to a loss of roll damping coupled with a strong spring.

From the results of the study at M = 0.8 and 0.9 for two δ_{LEF} deflections the following general conclusions are made. At three of the four conditions assessed, the SW2F configuration either eliminated uncommanded lateral activity or delayed it by 0.5° - 1°. For the fourth condition, $M = 0.9$ and $\delta_{LEF} = 15°$, the level of lateral activity for the baseline and SW2F configuration was indistinguishable for expected operational AoAs. In general, the SW2F increased static lateral stability over the baseline prior to stall. In the wing stall AoA range, the SW2F decreased C_{lp} while maintaining a strong $C_{l\beta}$. This caused large amplitude, high frequency wing rock to develop when the model was given a roll rate. The SW2F configuration delayed wing stall by 1°-2° but produced a sharp negative $C_{L\alpha}$. Also, the SW2F significantly reduced the level of rolling moment unsteadiness over the baseline as indicated by the C_{lrms} data.

B. Joint Strike Fighter

The CTOL and CV configurations of the JSF were tested over a large $M\text{-}\alpha\text{-}\beta\text{-}\delta_{LEF}$ space. In addition, several wing modifications were tested for the CV configuration including sealing the gap between the inboard and outboard LEF, adding VGs to the outboard portion of the wing, and reshaping the inboard face of the outboard LEF. The effects of deflecting the horizontal tails and TEFs were also investigated. The discussion of these modifications will cover the CTOL configuration first, followed by a review of the CV configuration.

1. CTOL Configuration

The CTOL configuration was evaluated using the FTR technique for $0.6 \le M \le 0.95$ and $\delta_{LEF} = 13°$, 16°, and 20°. In general, the uncommanded lateral activity for this configuration was benign. An example of the level of lateral activity of the CTOL model with $\delta_{LEF} = 16°$ is shown in Fig. 23. The plot shows little to no activity over the

tested Mach range. What activity that did exist was considered to be inconsequential as it was well off of the baseline flap schedule. The plot also presents a repeat point at $M = 0.9$ as an indication of the resolution of $p_{p\text{-}v}$. Figure 24 presents the FTR FOM for the three LEF deflections tested at $M = 0.8$ and shows that it would be relatively easy to schedule the LEF to avoid the limited regions of uncommanded lateral activity. CBSTAT evaluations conducted prior to the FTR test showed that the lateral aerodynamics of the CTOL were well behaved and absent of wing drop warning signs.. Based on these benign CBSTAT results, no modification was thought to be required for this variant so no alternate configurations were built for the model. The low-level of lateral activity on the FTR rig correlated well with these results and confirmed that wing drop was not likely to be a problem for the CTOL variant.

2. CV Configuration

a. Effect of Mach number

The CV model was tested over the Mach range $0.60 \le M \le 0.98$. At $M = 0.60$, the model did not exhibit any significant lateral activity for the configurations tested. At $0.70 \le M \le 0.92$, significant lateral activity was observed in the form of wing rock/drop. For $0.92 < M \le 0.96$, the model tended to trim at a large roll angle as a result of the lateral stability at these conditions. At some pitch attitudes, the model would trim at one ϕ for a period of time then abruptly change to trim at a significantly different ϕ. This unusual behavior was attributed to the fact that the stability of the configuration was neutral or slightly unstable at small sideslips but became stable as β increased. As the model rolled at a fixed θ, β increased until a trim point in C_l was achieved. Due to the weak lateral stability, even relatively small unsteady jumps in rolling moment could cause the model to transition to an entirely different trim point. For the limited cases that were obtained at $0.96 < M \le 0.98$, the model did not exhibit significant lateral activity and the static lateral stability was stable and more linear than at $0.92 < M \le 0.96$. For all of the Mach numbers tested, FTR results were consistent with the CBSTAT predictions developed from static test data taken in other tunnels prior to the test. The effect of Mach number just described holds true regardless of the modifications tested on the CV model.

b. Effect of Sealing the LEF Gap

During static force and moment testing on the JSF CV model, aerodynamic anomalies such as hysteresis, unsteadiness and poor repeatability were observed at several flight conditions. The regions exhibiting these unfavorable characteristics were initially identified using continuous β-sweep testing conducted as part of the CBSTAT wing drop evaluation technique. Once found, a variety of test methods including oil flow visualization, dwell testing and wing root bending moment analysis were used to further understand and isolate the source of these anomalies. Oil flow visualization of the upper wing surface was conducted for a range of sideslips. This showed that the problems were due primarily to a gap between the inboard and outboard LEFs that occurred at the wing fold location.

At some conditions it appeared that a vortex emanating from the LEF gap acted like a wing fence that prevented spanwise flow from the inboard section of the wing from degrading flow outboard of the wing fold. At specific combinations of Mach, α, and β the vortex would burst and the outer wing panel would stall abruptly resulting in a sudden change in rolling moment. At other conditions similar jumps in rolling moment were observed as a shock, which normally affixed itself near the TEF hinge-line, would migrate forward on the wing rapidly and attach itself to the LEF gap. When the shock jumped to the more forward position a significant reduction in lift would occur on the wing as the flow behind the shock was separated. Again, this sudden lift loss would produce rapid rolling moment changes that would undoubtedly lead to wing drop in flight.

On the FTR rig either of the two events described above would act as triggering mechanisms for the onset of lateral activity. The unsteady nature of these flow changes could be seen in the variety of roll motions observed during FTR testing. In some cases multiple large amplitude wing drops were observed as the model would roll suddenly to a large amplitude, return to zero bank, then experience another drop in the same, or opposite, direction. On other runs the model would sit quite still for extended periods of time before being upset by a sudden asymmetric rolling moment. At the most severe conditions the model would diverge immediately after brake release and exhibit large amplitude wing rock for the remainder of the time history.

Figure 25 shows the location and picture of the LEF gap. In general for $0.7 \le M \le 0.9$ and $10° \le \delta_{LEF} \le 20°$, the effect of sealing the gap was to reduce the severity and delay or eliminate the onset of significant lateral activity over the α-range tested. An example is shown in the FTR FOM plot of Fig. 26. The figure shows that the baseline wing has significant activity over the range $8° \le \alpha \le 16°$ (with the exception of $\alpha = 13°$ and 13.5°) which is classified as severe wing rock. At $\alpha = 8°$, 10°, 14°, and 15° the lateral activity occurred even from releasing the model at a $\phi_o = 0°$ initial condition. For $\alpha = 11°$, 12, and 16° the model did not show any significant lateral motion

when released from a wings level condition but did exhibit sustained, violent wing rock when the motion was initiated by releasing the model at a non-zero bank angle.

In general, the effect of sealing the gap and having a constant LEF deflection for the entire wing span reduced or eliminated unsteady rolling moments, decreased static lateral stability, increased roll damping, and caused an earlier break in the lift curve. The static lateral-stability, roll damping, and the type of lateral activity were similar for $9° \le \alpha \le 12°$. An example time history for these conditions is shown in Fig. 27 at $\theta = 10°$. The pronounced effect of sealing the LEF gap is easily seen by contrasting the severe wing rock of the baseline configuration with the new wing which shows no activity.

Insight into the aerodynamic causes of the baseline configuration lateral activity can be obtained from the static and dynamic data shown in Figs. 28 and 29. The C_l vs. β plot shown in Fig. 28 was collected during a series of continuous β-sweeps performed at constant α by sweeping from β = -10° to 10° then back again over the same range in the opposite direction. The plot shows that a large hysteresis loop exists for the baseline configuration between -4 and +3°β that are not present when the gap is sealed. These hysteresis loops indicate that there are multiple stable flow states at these conditions. This was confirmed by performing dwell testing inside these hysteresis loops which showed that multiple values of C_l can occur with no measurable variation in test condition. During FTR testing at $\alpha = 10°$ and $\phi_o = 0°$, the model immediately developed limit cycle wing rock (Fig. 27a) even though the model is statically stable for $-10° \le \beta \le 10°$ (which is the range of β experienced during the wing rock). This behavior is explained by the combined effect of the unsteady, multi-valued rolling moments at low β and the unstable C_{lp} at $\alpha = 10°$ shown in Fig. 29. After being released at $\phi_o = 0°$ the model evidently experienced an asymmetric flow topology change which triggered the rolling motion. Once started, a limit cycle wing rock ensues due to the unstable roll damping near $\beta = 0°$, stable $C_{l\beta}$, and a forcing function shown by the hysteresis loop shown in Fig. 28.

Further examination of Figs. 28 and 29 can also explain why the baseline configuration showed much lower levels of lateral activity around $\alpha = 13°$ than in the 8° to 12° region in Fig. 26. Unlike the other α's shown, the $\alpha = 13°$ data in Fig. 28 does not exhibit any hysteresis for the open gap configuration near $\beta = 0°$. In addition, Fig. 29 shows that the baseline configuration has marginal dynamic stability around $\alpha = 13°$. Therefore, the static and dynamic data support the absence of significant activity at $\alpha = 13°$ seen on the FTR rig when the model is released with no roll rate at an initial condition of $\beta = \phi = 0°$. However, since hysteresis loops do exist beyond $\beta = \pm 2.5°$ and C_{lp} is nearly neutral, the possibility for lateral activity does exist and may well occur if the baseline configuration were given a roll rate by releasing it at a non-zero ϕ. Unfortunately, a bank and release run was not performed at this test condition.

As shown in the FTR FOM plot of Fig. 26, the new wing has no significant lateral activity except at $\alpha = 13°$. Relative to the baseline, the new wing also eliminates the hysteresis loops in static rolling moment (Fig. 28) and increases roll damping (Fig. 29) significantly except at $\alpha = 13°$. Based on these changes it appears that the FTR activity at $\alpha = 13°$ can be attributed to the nonlinearities in rolling moment near $\beta = 0°$ (Fig. 28) and the localized reduction in roll damping at this condition.

To further understand the effect of the gap, sensitivity to the chordwise length of the gap was briefly evaluated using continuous pitch-up sweeps. For this investigation the width of the gap was not varied but it was filled in starting from the downstream end such that approximately two-thirds of the gap was closed. The FTR FOM results in Fig. 30 for $0.70 \le M \le 0.90$ show that the level of lateral activity is highly sensitive to the gap depth. This finding indicates that a robust design that completely seals the gap is required to avoid wing drop. Note that the summary shown in Fig. 30 presents the maximum value of $p_{p\text{-}v}$ for the entire pitch sweep range rather than the pitch-pause points that are normally used when calculating $p_{p\text{-}v}$. Continuous pitch-up sweeps were used frequently during the test as a means of quickly screening a new configuration. The FTR FOM plot does not show at which θ the peak $p_{p\text{-}v}$ value occurred at but this θ was approximately the same for both configurations at each Mach that was evaluated. The reason for using the FOM plot rather than showing roll angle time history plots is that it succinctly captures the effect of partially sealing the gap for $0.7 \le M \le 0.90$. It would require the use of twelve time history plots to show the breadth of information contained in this one plot.

c. Effect of LEF gap geometry

The inward face of the outboard LEF was flat for the results shown above. For the full scale aircraft this face would be beveled so a short investigation of this geometry change was performed. Figure 31 shows the effect of the beveled flap edge on the lateral activity for $0.6 \le M \le 0.9$ with $\delta_{LEF} = 12.5°$ using the FTR FOM. The $p_{p\text{-}v}$ is computed from continuous pitch-up sweeps using the maximum value of $p_{p\text{-}v}$ over the entire pitch range. As the plot shows there is no effect of the beveled edge except at $M = 0.9$ where the value of $p_{p\text{-}v}$ is twice that for the flat face.

d. Effect of Vortex Generators (VGs)

One alternative to sealing the gap, which showed some promise in static wind tunnel testing, involved placing three VGs on the outer wing panel. Figure 32 presents the effect of VGs on the lateral activity along with a picture showing the location of the VGs as viewed looking outboard along the left wing. The $p_{p\text{-}v}$ is computed from continuous pitch-up sweeps using the maximum value of the $p_{p\text{-}v}$ over the entire pitch range. Results indicate that the VGs actually cause significant increases in the lateral activity at $M = 0.60$ and 0.90, have no effect at $M = 0.70$ and 0.85, and provide only a minor reduction in the level of lateral activity at $M = 0.80$. Based on these results, and the mixed data that was obtained during conventional force and moment testing, the VGs were considered to be a non-viable solution.

e. Effect of Horizontal Tail Deflection

Nearly all of the FTR testing was done with the horizontal tails set to zero degrees deflection but a short test series was done to determine the effect of horizontal tail deflection on the level of lateral activity. Given the tail's close proximity to the wing (see sketch in Fig. 25), there was some concern that horizontal tail deflections may influence the wing aerodynamics thereby aggravating wing drop characteristics. Figure 33 shows the effect of symmetric horizontal tail deflections on the lateral activity for $0.7 \leq M \leq 0.90$ with the LEF gap sealed and $\delta_{LEF} = 10°$. The $p_{p\text{-}v}$ values, which again represent the maximum $p_{p\text{-}v}$ value observed during continuous pitch-up sweeps, show that deflecting the tail either decreases or has no considerable effect on the level of lateral activity. Therefore, assessing the wing drop tendencies of the model with the horizontal tails undeflected is a conservative approach.

f. Flap Scheduling

Since sealing the LEF gap did not completely eliminate the potential for wing drop/rock over the entire α-range, some scheduling of the flaps will be required to avoid problem areas. Figure 34 shows the level of lateral activity, expressed as $p_{p\text{-}v}$, for three LEF deflections at $M = 0.70$, 0.80, 0.85, 0.90. The plots clearly show that the peaks in lateral activity spread out in a predictable pattern with LEF deflection. As with the CTOL variant, these results indicate that a reasonable schedule can be developed for the CV configuration to avoid flight conditions exhibiting significant levels of lateral activity.

IV. Summary

The objective of this paper was to analyze the effect of configuration changes on the FTR activity of an 8% pre-production F/A-18E and a 1/15th scale F-35 at transonic speeds. These models were tested in the NASA Langley 16-Foot Transonic Tunnel. The modifications analyzed include leading and trailing edge flap deflections, fences, sealing the LEF gap, and vortex generators. The analysis used a modification of the FTR figure-of-merit developed during the Abrupt Wing Stall Program to discern configuration effects. The severity of the uncommanded lateral activity as measured by the FTR technique was correlated with the static force and moment data.

The study of the pre-production F/A-18E involved comparing the baseline configuration to a modification consisting of changing the LEF shape at the wing fold fairing and adding two wing fences. Based on the results of this study for 0.8 and 0.9 Mach with two δ_{LEF} deflections the following observations are made. At three of the four conditions assessed, the modified configuration either eliminated uncommanded lateral activity or delayed it by 0.5° - 1°. For the fourth condition, $M = 0.9$ and $\delta_{LEF} = 15°$, the level of lateral activity for the baseline and modified configuration was indistinguishable for expected operational AoAs. The modified configuration increased static lateral stability over the baseline prior to stall. In the wing stall AoA range, the modified configuration decreased C_{lp} while maintaining a strong $C_{l\beta}$. This caused large amplitude, high frequency wing rock to develop when the model was given a roll rate. The modified configuration delayed wing stall by 1°-2° but produced a sharp negative $C_{L\alpha}$. Also, the modified configuration significantly reduced the level of rolling moment unsteadiness over the baseline as indicated by the C_{lrms} data.

For the JSF model, data from both the CTOL and CV variants were analyzed. The results of the CTOL variant FTR tests confirmed that this configuration does not exhibit uncommanded lateral activity on the nominal flap schedule. Even off schedule conditions showed only moderate activity for a few $M\text{-}\alpha\text{-}\delta_{LEF}$ combinations. For the CV configuration, static wind tunnel testing done previously using CBSTAT had indicated that the baseline configuration was prone to wing drop at several conditions. Therefore both the baseline and a modified wing configuration, developed based on CBSTAT evaluation, were tested. The principle change in the modified configuration was to seal the gap between the inboard and outboard LEF. To implement this seal a change was made to the LEF hinge-line and the inboard and outboard LEFs were scheduled to the same deflection. Although these changes are more obvious than the sealing of the gap, they did not contribute to the improvement in lateral characteristics. In general, sealing the LEF gap reduced or eliminated unsteady rolling moments, decreased static

lateral stability, increased roll damping, and caused an earlier break in the lift curve. As predicted based on CBSTAT analysis, the FTR results confirmed that the baseline wing had unacceptable FTR activity and that sealing the gap resolved the majority of these issues. The effect of the geometry inside the gap was also investigated and proved to have little effect on lateral activity except at $M = 0.90$. Vortex generators were investigated and found to be ineffective. Symmetric horizontal tail assessments showed that deflecting the tail decreased or had no considerable effect on the level of lateral activity. Finally, it was shown that LEF scheduling could be used to avoid any potential uncommanded lateral activity based on the FTR FOM results.

Acknowledgements

Mrs. Naomi McMillian, Mr. Fran Capone and Mr. Kevin Cunningham of NASA – LaRC and Dr. Steve Cook of Naval Air Systems Command (NAVAIR), Patuxent River provided assistance with the wind tunnel tests. For the pre-production F/A-18E test The Boeing Company provided the model and additional test support personnel.

References

[1]Chambers, J., and Hall, R., "Historical Review of Uncommanded Lateral-Directional Motions at Transonic Conditions," *Journal of Aircraft*, Vol. 41, No. 3, 2004, pp. 436-447.

[2]Kashafutdinov, and S., Derishev, S., "Major Scientific Areas and Experimental Facilities of Sibnia Aerodynamic Research and Development Division.

[3]Hwang, C., and Pi, W., "Some Observations on the Mechanism of Aircraft Wing Rock," AIAA Paper 78-1456, Aug. 1978.

[4]Hall, R., and Woodson, S., "Introduction to the Abrupt Wing Stall (AWS) Program," *Journal of Aircraft*, Vol. 41, No. 3, 2004, pp. 425-435.

[5]McMillin, N., Hall, R., and Lamar, J., "Understanding Abrupt Wing Stall with Experimental Methods," AIAA Paper 2003-0591, Jan. 2003.

[6]Woodson, S., Green, B., Chung, J., Grove, D., Parikh, P., and Forsythe, J., "Understanding Abrupt Wing Stall (AWS) with CFD," AIAA Paper 2003-0592, Jan. 2003.

[7]Schuster, D., and Byrd, J., "Transonic Unsteady Aerodynamics of the F/A-18E at Conditions Promoting Abrupt Wing Stall," *Journal of Aircraft*, Vol. 41, No. 3, 2004, pp. 485-492.

[8]Forsythe, J., and Woodson, S., "Unsteady CFD Calculations of Abrupt Wing Stall Using Detached-Eddy Simulation," AIAA Paper 2003-0594, Jan. 2003.

[9]Parikh, P, and Chung, J., "A Computational Study of the AWS Characteristics for Various Fighter Jets: Part I, F/A-18E & F-16C," AIAA Paper 2003-0746, Jan. 2003.

[10]Chung, J., and Parikh, P., "A Computational Study of the Abrupt Wing Stall (AWS) Characteristics for Various Fighter Jets: Part II, AV-8B and F/A-18C," AIAA Paper 2003-0747, Jan. 2003.

[11]Lamar, J., Capone, F., and Hall, R., "AWS Figure of Merit (FOM) Developed Parameters from Static, Transonic Model Tests," AIAA Paper 2003-0745, Jan. 2003.

[12]Lamar, J., Hall, R., Capone, F., and McMillin, N., "Usefulness of Transonic Model Static Data in Predicting Flight Abrupt-Wing-Stall," *Journal of Aircraft*, Vol. 41, No. 3, 2004, pp. 464-473.

[13]Capone, F; Owens, B., and Hall, R., "Development of a Free-To-Roll Transonic Test Capability," *Journal of Aircraft*, Vol. 41, No. 3, 2004, pp. 456-463.

[14]Owens, B., Capone, F., Hall, R., Brandon, J., Cunningham, K., and Chambers, J., "Transonic Free-To-Roll Analysis of Abrupt Wing Stall on Military Aircraft," *Journal of Aircraft*, Vol. 41, No. 3, 2004, pp. 474-484.

[15]Roesch, M., and Randall, B., "Flight Test Assessment of Lateral Activity," AIAA paper 2003-0748, Jan. 2003.

[16]Green, B., and Ott, J., "F/A-18C to E Wing Morphing Study for the Abrupt Wing Stall Program," AIAA Paper 2003-0925, Jan. 2003.

[17]Kokolios, A., and Cook, S., "Use of Piloted Simulation for Evaluation of Abrupt Wing Stall Characteristics," AIAA Paper 2003-0924, Jan. 2003.

[18]Capone, F., Hall, R.; Owens, B., Lamar, J., and McMillin, N., "Review and Recommended Experimental Procedures for Evaluation of Abrupt Wing Stall Characteristics," *Journal of Aircraft*, Vol. 41, No. 3, 2004, pp. 448-455.

[19]Woodson, S., Green, B., Chung, J., Grove, D., Parikh, P., and Forsythe, J., "Recommendations for CFD Procedures for Predicting Abrupt Wing Stall (AWS)," AIAA Paper 2003-0923, Jan. 2003.

[20]Cook, S., Chambers, J., Kokolios, A., Niewoehner, R., Owens, B., Page, A., and Roesch, M., "An Integrated Approach to Assessment of Abrupt Wing Stall for Advanced Aircraft," AIAA Paper 2003-0926, Jan. 2003.

[21]Hall, R., Woodson, S., and Chambers, J., "Accomplishments of the AWS Program and Future Requirements," AIAA Paper 2003-0927, Jan. 2003.

[22]McConnell, J., "Continuous Beta Sweep Test and Analysis Technique (CBSTAT) for Predicting Wing Drop Based on Static Wind Tunnel Testing," AIAA Paper 2004-5048, Aug. 2004.

[23]Kokolios, A., Gonzalez, H., Ghee, T., and Pettersson, H., "Analysis of Beta Hysteresis Figure of Merit on a Super Hornet Configuration," AIAA Paper 2004-5051, Aug 2004.

[24]Payne, P., and McConnell, J., "Predicting Wing Drop on the Harrier II Using the Static Wind Tunnel Test and Analysis Technique CBSTAT," AIAA Paper 2004-5050, Aug 2004.

[25]Cook, S., Gonzalez, H., Owens, B., McConnell J., and Payne, P., "Correlation of the Continuous Beta Sweep Test and Analysis Technique to Transonic Free-to-Roll and Flight Test Results," AIAA Paper 2004-5052, Aug 2004.
[26]Wolowicz, C. H., Bowman, J. S., and Gilbert, W. P., "Similitude Requirements and Scaling Relationships as Applied to Model Testing," NASA TP 1435, 1979.
[27]Brandon, J., and Foster, J., "Recent Dynamic Measurements and Considerations for Aerodynamic Modeling of Fighter Airplane Configurations," AIAA Paper 98-4447, Aug. 1998.
[28]Morelli, E., "System IDentification Programs for AirCraft (*SIDPAC*)," AIAA paper 2002-4704, Aug. 2002.

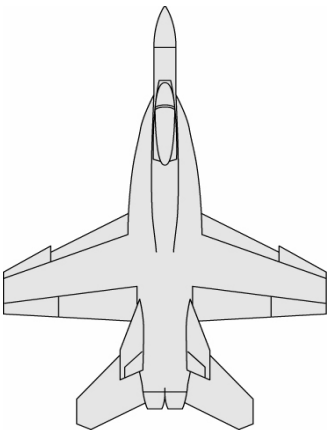

Figure 1. Sketch of the 8% F/A-18E baseline model. S_{ref} = 3.2 ft^2, b_{ref} = 3.34 ft., c_{ref} = 1.048 ft.

Figure 2. Sketch of the 1/15th scale baseline CV model of the JSF. S_{ref} =2.76 ft^2, b_{ref}=2.87 ft., c_{ref} = 1.113 ft.

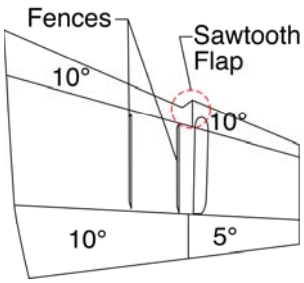

Figure 3. Sketch of the F/A-18E wing showing the saw-tooth LEF and the location of the fences.

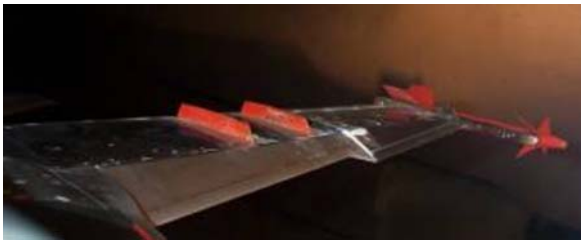

Figure 4. Picture of the saw-tooth LEF and the wing fences looking out the port wing of the 8% F/A-18E model.

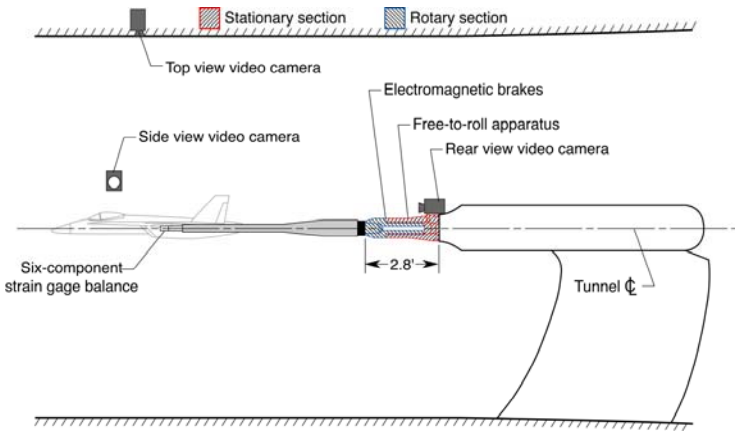

Figure 5. Sketch of the NASA Langley 16-ft TT FTR apparatus.

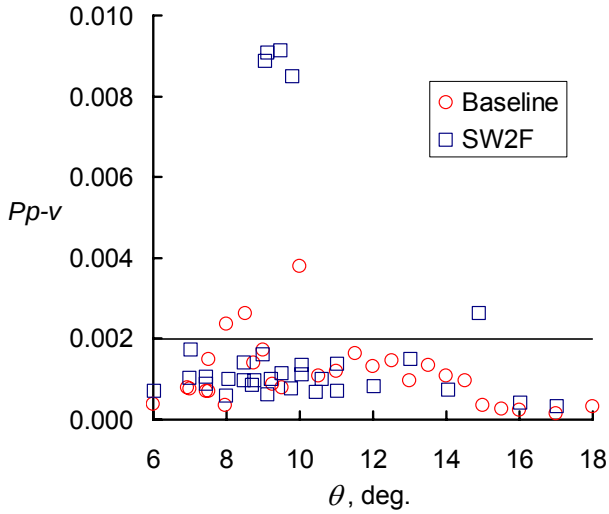

Figure 6. Lateral activity of the 10/10/5 Baseline and SW2F configurations at M = 0.8

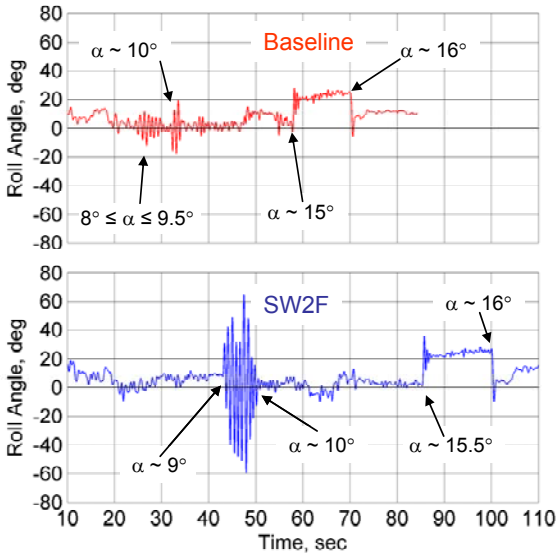

Figure 7. Roll angle time history of the 10/10/5 Baseline and SW2F configurations during a continuous pitch-up sweep at M = 0.8.

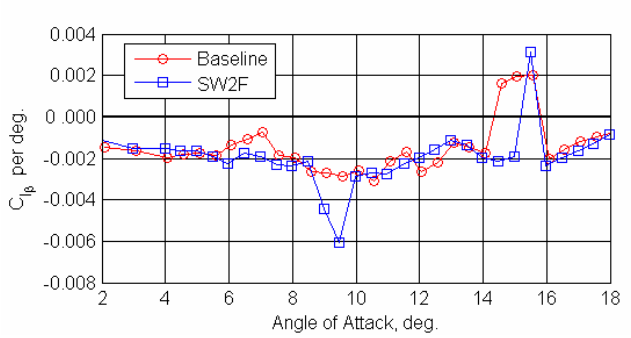

Figure 8. Static lateral stability about $\beta = 0°$ for the 10/10/5 baseline and SW2F configurations at $M = 0.8$.

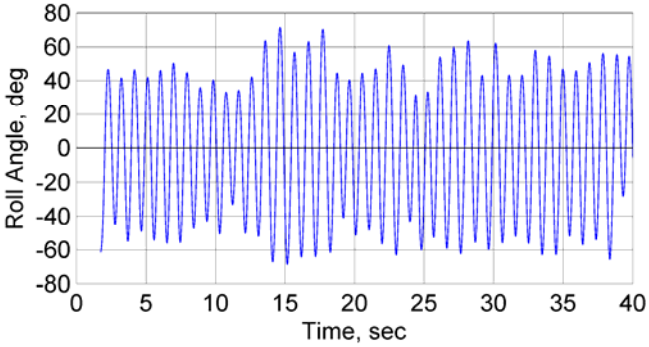

Figure 9. 10/10/5 SW2F configuration with initial $\phi = -60°$, $\theta = 9°$, and $M = 0.8$

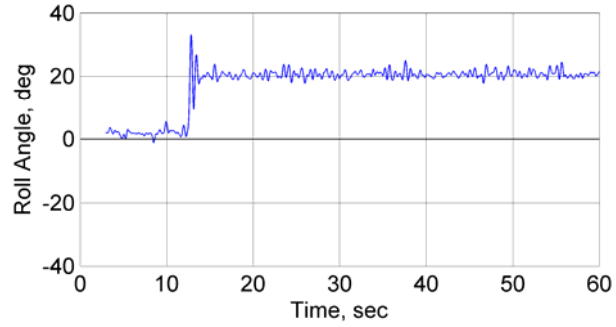

Figure 10. Roll angle time history of the 10/10/5 SW2F configuration at $\theta = 15°$ and $M = 0.8$.

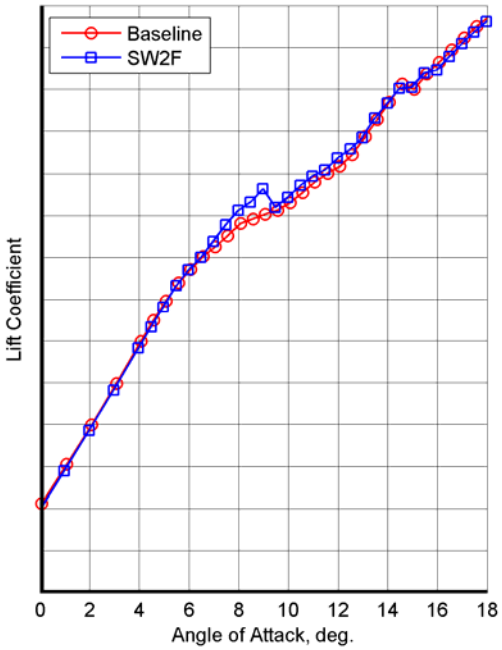

Figure 11. Lift characteristics for the 10/10/5 Baseline and SW2F configurations at M = 0.8.

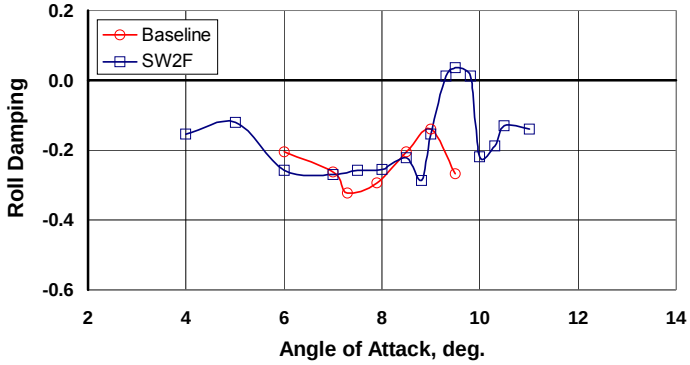

Figure 12. Roll damping for the 10/10/5 baseline and SW2F configurations at $M = 0.8$.

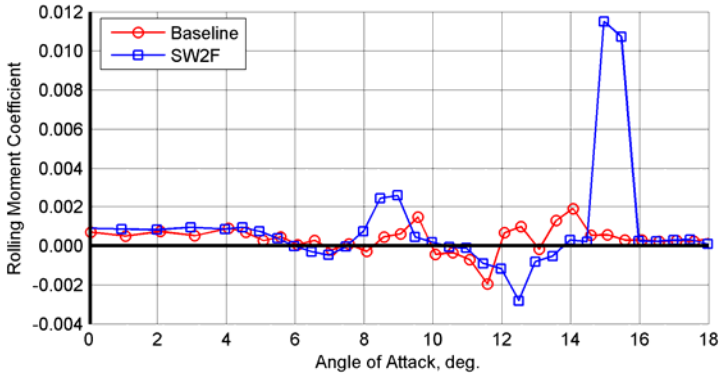

Figure 13. Rolling moment characteristics of the 10/10/5 Baseline and SW2F configurations at $\beta = 0°$ and $M = 0.8$.

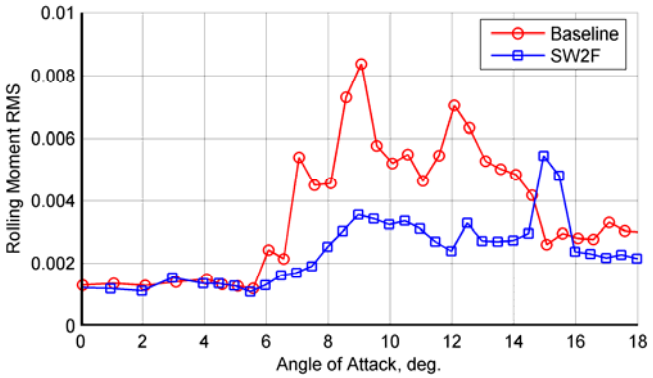

Figure 14. Rolling moment rms characteristics of the 10/10/5 Baseline and SW2F configurations at $\beta = 0°$ and $M = 0.8$.

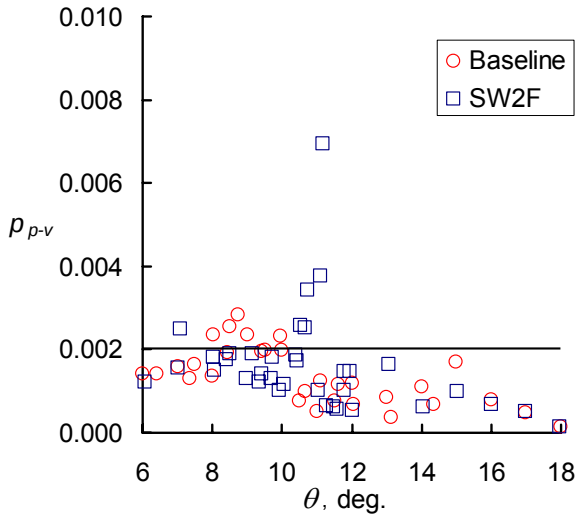

Figure 15. Lateral activity of the 10/10/5 Baseline and SW2F configurations at $M = 0.9$.

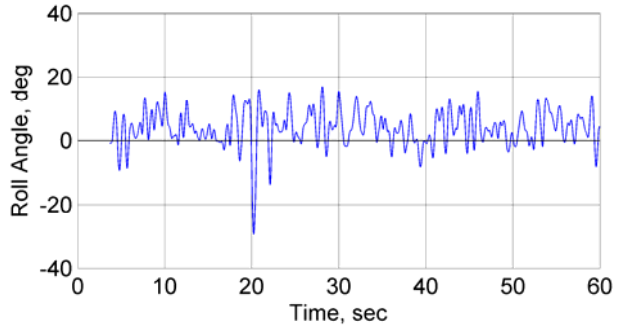

Figure 16. Roll angle time history of the 10/10/5 SW2F configuration at $\theta = 7°$ and $M = 0.9$

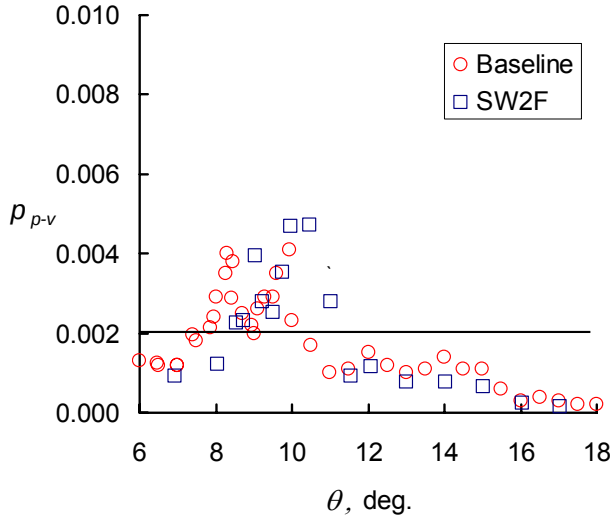

Figure 17. Lateral activity of the 15/10/5 Baseline and SW2F configurations at M = 0.8.

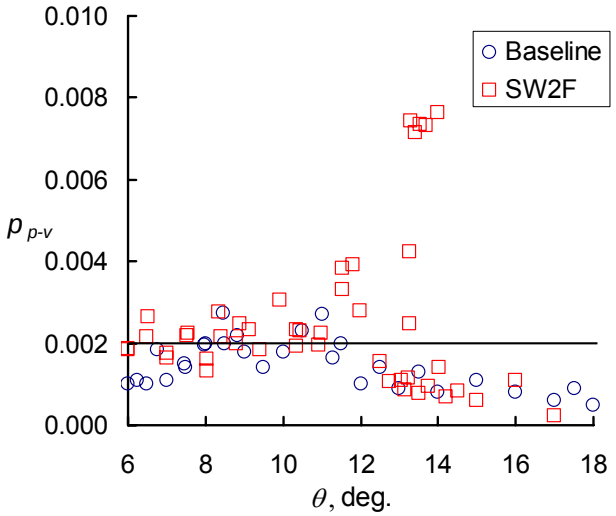

Figure 18. Lateral activity of the 15/10/5 Baseline and SW2F configurations at M = 0.9.

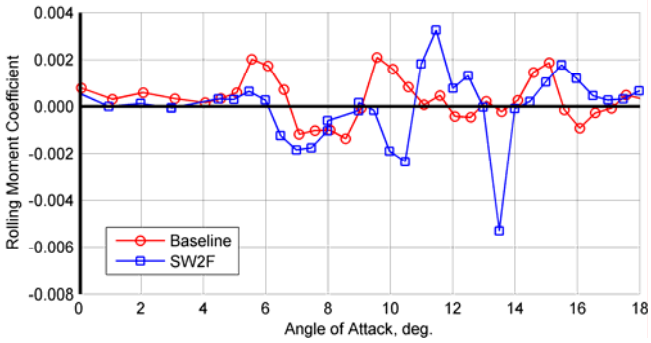

Figure 19. Rolling moment for the baseline and SW2F configurations with 15/10/5 flap settings at *M* = 0.9.

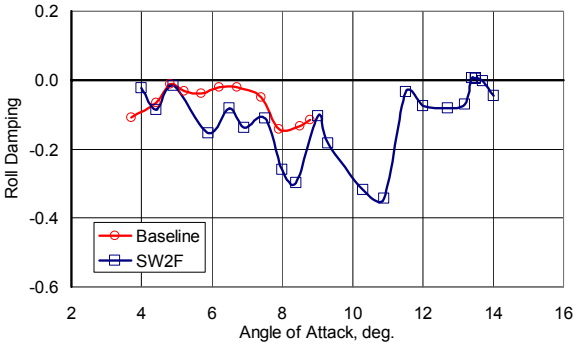

Figure 21. Roll damping for the 15/10/5 baseline and SW2F configurations at *M* = 0.9.

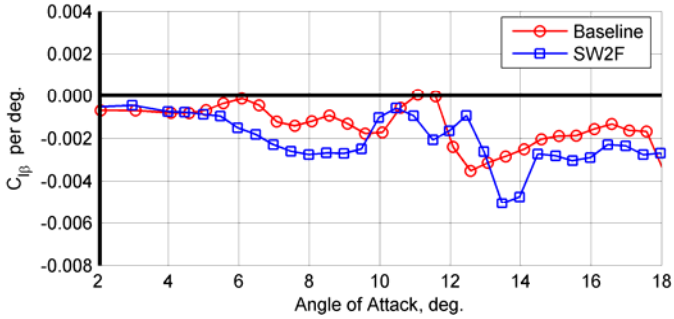

Figure 20. Static lateral stability for the 15/10/5 Baseline and SW2F configurations at *M* = 0.9.

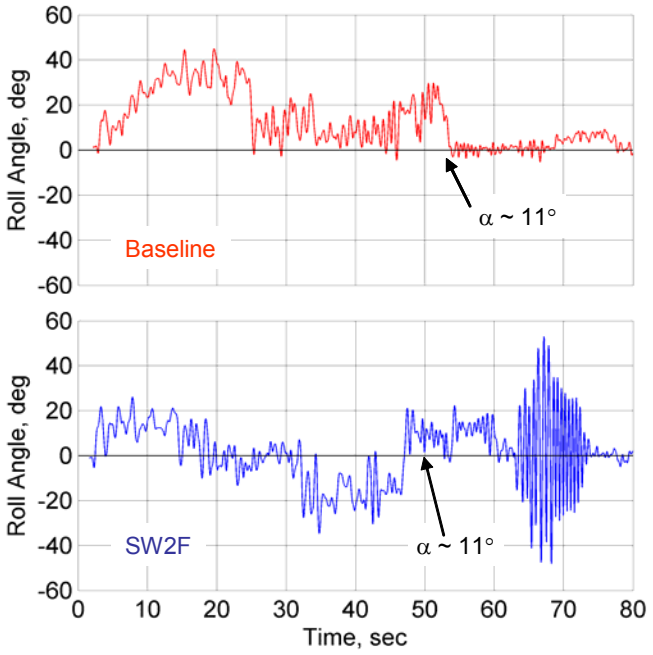

Figure 22. Roll angle time history during a continuous pitch-up sweep for the 15/10/5 baseline and SW2F configurations at $M = 0.9$.

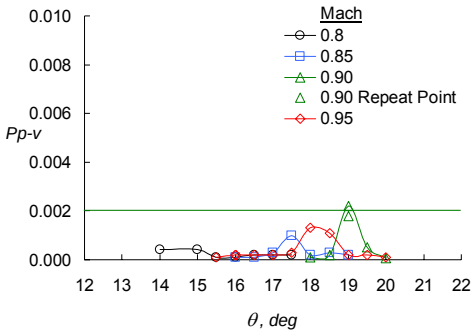

Figure 23. Effect of Mach number on the lateral activity of the CTOL configuration for $\delta_{LEF} = 16°$.

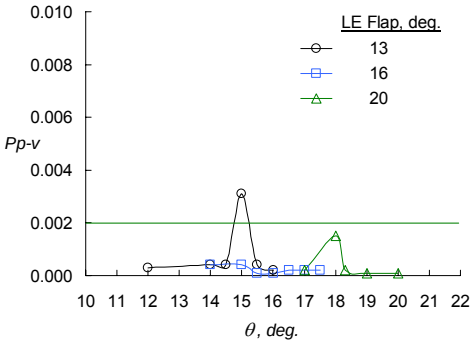

Figure 24. Effect of flap deflection on the lateral activity of the CTOL configuration for $M = 0.8$.

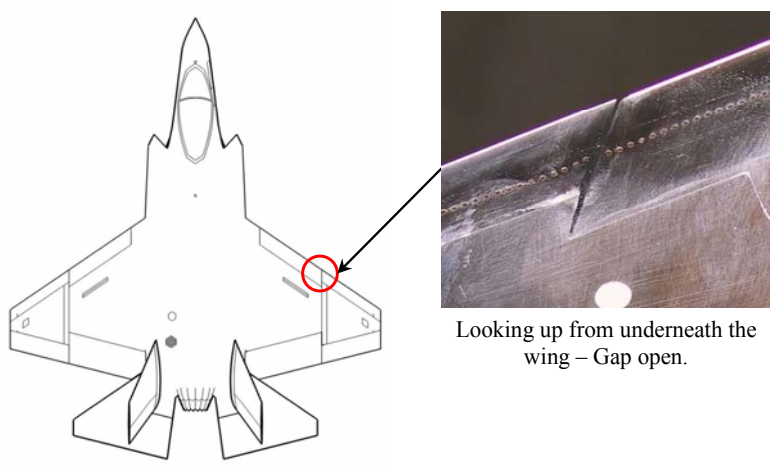

Figure 25. Sketch of JSF CV model showing the gap between the inboard and outboard LEF. Also shown are the trip dots.

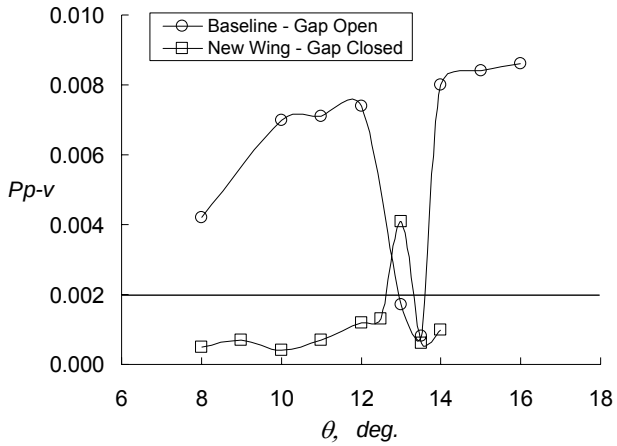

Figure 26. Effect of sealing the gap on the lateral activity of the JSF CV model at M = 0.85 (Baseline: δ_{LEF} = 12.5°/15.5°; New wing: δ_{LEF} = 12.5°).

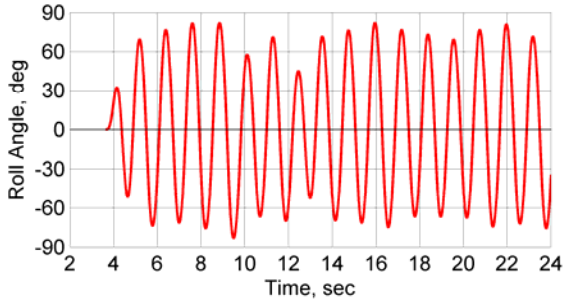

Figure 27a Roll angle time history of the baseline with δ_{LEF} = 12.5°/15.5° at θ = 10° and M = 0.85

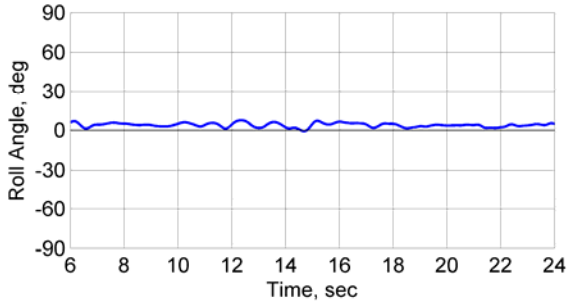

Figure 27b Roll angle time history of the new wing with δ_{LEF} = 12.5° at θ = 10° and M = 0.85

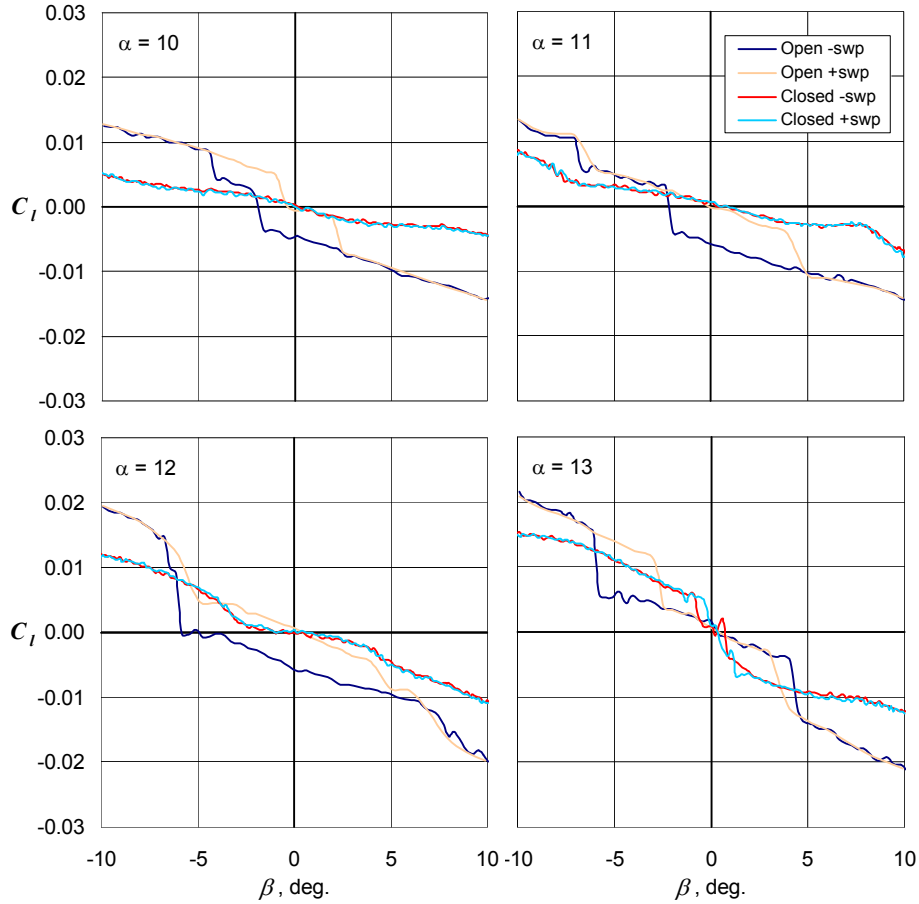

Figure 28. Static rolling moment for the open gap case (baseline wing with δ_{LEF} = 12.5°/15°) and sealed gap case (new wing with δ_{LEF} = 12.5°) at M = 0.85.

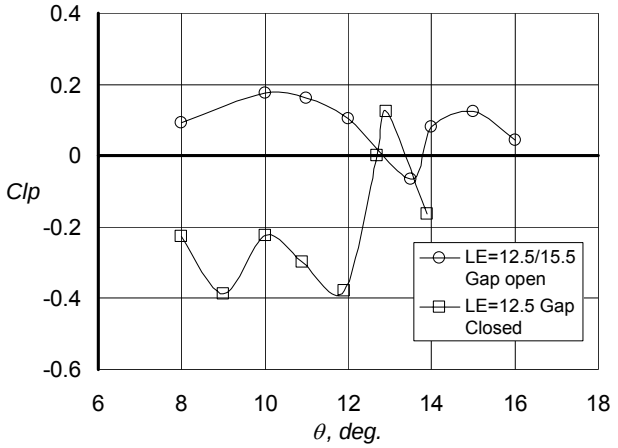

Figure 29. Roll damping for the baseline (δ_{LEF} = 12.5/15.5) and new wing (δ_{LE} = 12.5) at M = 0.85.

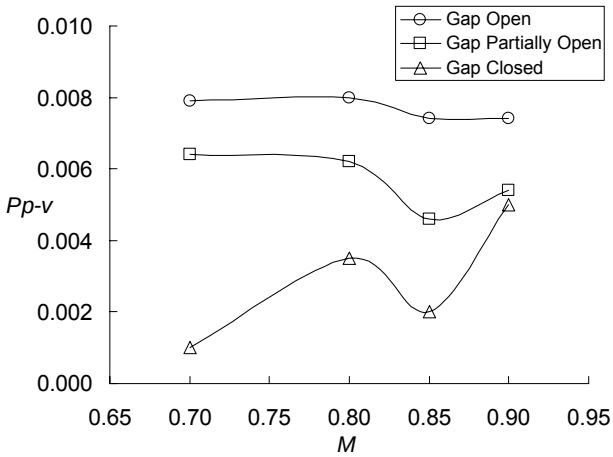

Figure 30. Effect of partially sealing the gap. New wing with δ_{LEF} = 12.5°.

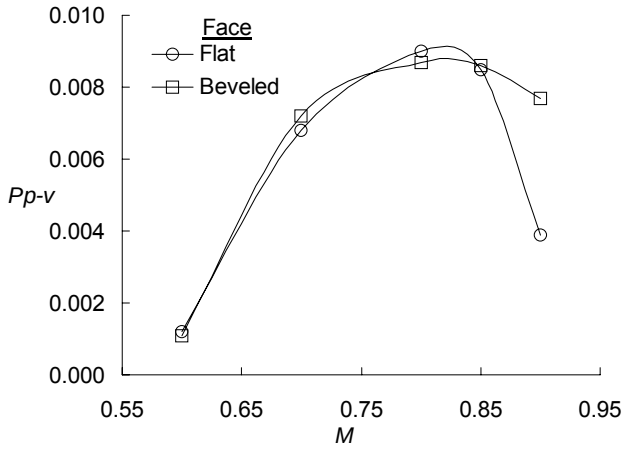

Figure 31 Effect of beveling the inboard face of the outboard LEF on the lateral activity for the baseline wing with a δ_{LEF} = 12.5°/15.5°.

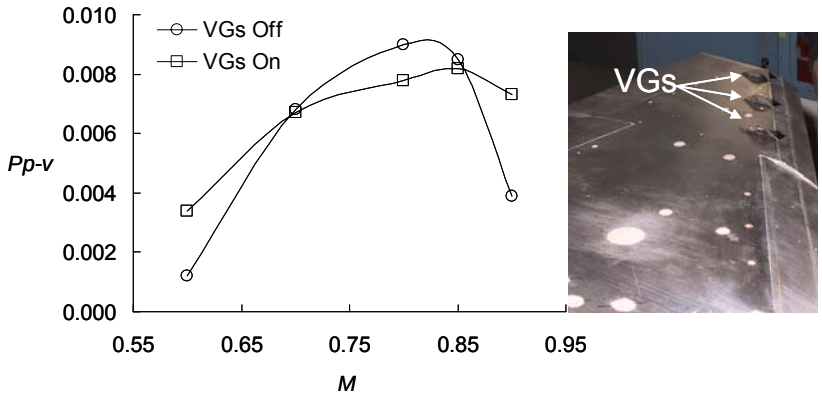

Figure 32 The effect of VGs on the lateral activity for $0.60 \le M \le 0.90$ and δ_{LEF} = 12.5/15.5. Inset - looking out the left wing showing the location of the three VGs.

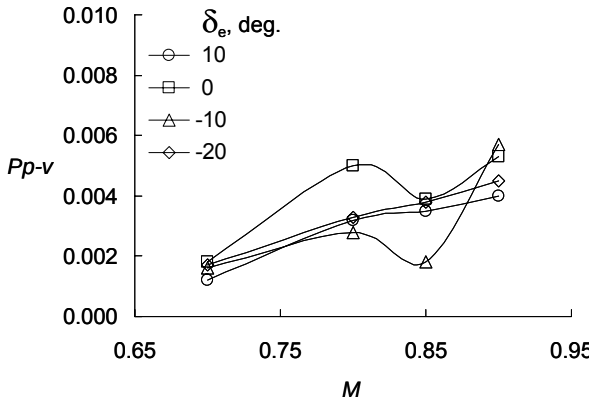

Figure 33 Effect of horizontal tail deflection on the lateral activity of the new wing with δ_{LEF} = 10°. LEF gap sealed.

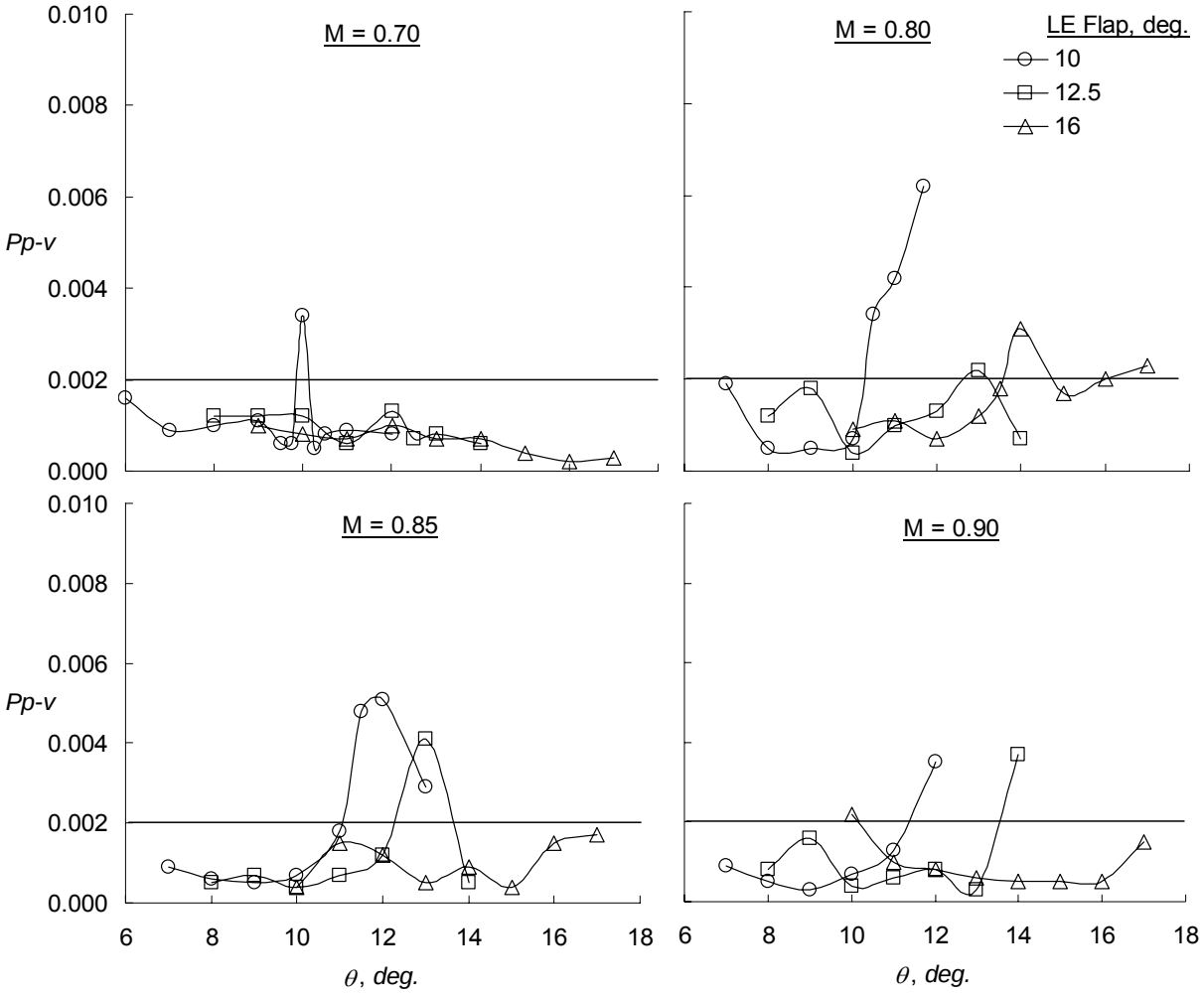

Figure 34 Use of the FTR-FOM for determining flap schedule at M = 0.70, 0.80, 0.85, and 0.90.